Composites Part B xxx (2017) xxx-xxx

Contents lists available at ScienceDirect

Composites Part B

journal homepage: www.elsevier.com

Experimental investigation on cyclic response of RC elements repaired by CFRP external reinforcing systems

Francesco Capani [a], Angelo D'Ambrisi [a], Mario De Stefano [a], Francesco Focacci [b, *], Raimondo Luciano [c], Raffaele Nudo [a], Rosa Penna [d]

[a] Dipartimento di Architettura, Università di Firenze, Piazza Brunelleschi 6, 50121 Firenze, Italy
[b] Università eCampus, Via Isimbardi 10, 22060 Novedrate, CO, Italy
[c] Dipartimento di Meccanica, Strutture, Ambiente e Territorio, Università di Cassino e del Lazio Meridionale, Viale dell'Università, 03043 Cassino, FR, Italy
[d] Dipartimento di Ingegneria Civile, Università di Salerno, Via Ponte Don Melillo, 84084 Fisciano, SA, Italy

ARTICLE INFO

Article history:
Received 20 December 2016
Accepted 30 December 2016
Available online xxx

Keywords:
RC buildings
Experimental investigation
Cyclic response
Seismic damage
Repair
CFRP wrapping

ABSTRACT

This paper deals with the experimental results of an investigation aimed at studying cyclic response of half scaled RC specimens previously damaged and then repaired with externally bonded carbon fiber reinforced polymer sheets. The research involved the test of ten specimens. Two of them were tested without any external strengthening material in order to provide a reference for the response of repaired specimens. These latter were tested after a previous damaging procedure and a subsequent repair intervention with fiber reinforced polymer composites. The parameters under investigation were the level of initial damage, the strengthening configuration, and the level of axial load. Test results have pointed out effectiveness of the adopted strengthening systems, since repaired specimens exhibited better mechanical responses than the unstrengthened ones.

1. Introduction

A huge number of reinforce concrete (RC) buildings in seismic areas were designed for gravity loads only or according to early codes without requirements on ductile reinforcement detailing. These buildings exhibit seismic capacity lower than the seismic demand provided by current codes. In particular, recent earthquakes highlighted the vulnerability of the beam-column joints in moment resisting frames. Typically, these frames suffer of inadequate transverse reinforcement within the beam-column joints and inadequate anchor length of the longitudinal steel rebars crossing the joints. In addition, columns of RC frames are particularly sensitive to seismic actions and suffer more or less severe damage even for earthquakes having a medium-low intensity. Besides, it is possible that the suffered damage is quite different at column ends, as it often happens to first level columns of frame structures. Furthermore, it is recognized that the performance of beam-column joints affects the overall seismic response of reinforced concrete frame structures. Therefore, it is necessary to develop and assess the effectiveness of economical techniques to strengthen the beam-column joints and repair those damaged by seismic events.

The strengthening of beam-column joints involves the shear strengthening of beams and columns in the critical regions, the confinement of the column ends and the improvement of the bond-slip behavior of the longitudinal steel rebars in order to avoid brittle shear failure modes and promote a ductile flexural failure mode. Several techniques were proposed for enhancing the seismic response of beam-column joints and repairing beam-column joints damaged by seismic events. Most of them are based on the use of steel [1,2] or reinforced concrete [3–6] jackets. Although these techniques proved their effectiveness for improving the beam-column joint capacity in terms of strength and ductility, their extensive application is limited by architectural restrictions, since increase of the dimensions of the structural elements is needed.

The issues of upgrading buildings with structural deficiencies and repairing structures damaged by seismic events determined in recent years a growing interest among scientific community and structural engineers towards fiber reinforced polymer (FRP) composites. This is confirmed by the several practical applications on RC [7], masonry [8–11], and timber [12] structures and by issuing of specific technical guidelines in many countries [13–16]. Several researches have shown the effectiveness of FRP composites for strengthening of beam-column joints in terms of shear strength and energy dissipation capacity [17–20]. The overall structural ductility also increases, since the failure mode can be shifted from the joint to the adjacent members. Furthermore, the members failure mechanism can be modified from shear to flexure, fulfilling the requirements of modern codes on strength hierarchy. Two types of specimens are mainly tested by researchers to simulate beam-column joints, namely T shaped specimens [17,18], and cross specimens [19]. The beneficial effect of FRP materials application on the seismic capacity of a full scale frame was studied in Ref. [20] by means of pseudodynamic tests. Since the debonding of composite material from the support is recognized as the typical failure mode of FRP strengthened concrete and masonry

* Corresponding author.
Email address: francesco.focacci@uniecampus.it (F. Focacci)

http://dx.doi.org/10.1016/j.compositesb.2016.12.053
1359-8368/

structures [9-11,21-25], the strengthening setup adopted by some researchers involved the adoption of bolted steel plates in an attempt to provide a mechanical anchorage of the composite material [17,18]. Two main topics have been addressed by researchers: (i) use of FRP composites for strengthening beam-column joints of RC frames with inadequate reinforcement detailing [26], and (ii) use of FRP composites for repairing beam-column joints of RC frames with inadequate reinforcement detailing and damaged by a previous seismic event [17–20].

In this paper, this last topic is addressed. Based on previous remarks, an experimental campaign has been developed at the laboratory for tests on materials and structures (LPMS) of the University of Florence, aimed at studying the cyclic response of RC specimens previously damaged and then repaired with carbon fiber reinforced polymer (CFRP) composites. Eight specimens, each one representing two columns, have been damaged and then repaired with different configurations of FRP composites. The experimental program was planned to test ten specimens, including two control specimens, conceived according to the following study variables. 1. Level of initial damage: specimens have been initially subjected to two different damage levels, then repaired with FRP composites, and subjected to a cyclic load; 2. Type of repair system: different external strengthening configurations were adopted combining the application of unidirectional and quadriaxial fiber sheets; 3. Intensity of axial load applied to the column: two different levels of axial load have been considered. The amount of steel reinforcement as well as mechanical properties of materials have been kept constant for all the specimens. Since it is possible that the suffered damage is quite different at column ends, as it often happens to first level columns of frame structures, the repair intervention of real structures may be executed using different strengthening configurations at the column ends. In this case, if a new earthquake occurs, the repaired structure may experience unexpected structural behavior due to the asymmetry of the repair work. In order to investigate this aspect, some of the adopted strengthening configurations involve different strengthening setups at the column ends.

2. Experimental program

2.1. Test configuration and specimens geometry

Fig. 1a and b illustrates the test configuration, geometry of specimens and arrangement of longitudinal and transverse steel reinforcement.

Each specimen represents of two column elements having a rectangular cross section of 100 mm × 200 mm and a length of 800 mm. Each column has a shear span to cross-section depth ratio typical of short elements for which the shear failure mechanism plays a fundamental role in the mechanical response. The two column elements are connected each other and to the reaction frame by means of concrete stubs of 100 mm × 300 mm × 200 mm. Constraint conditions are accomplished by mechanical devices applied to the end stubs. These devices are capable of releasing axial deformation and opposing rotations [27]. At the top of the central stub, a mechanical actuator is mounted to provide the transverse action under displacement control. By this way each column element is subjected, during the test, to linear double-curvature flexure and constant shear force. The constraint degree provided at the end blocks can be modified to obtain different values of bending moment at end cross-sections of each column element. Besides, the overall symmetry of the test configuration allows to average, in the same test, the responses of two column elements having identical characteristics as regards geometry and mechanical properties. Longitudinal steel reinforcement consists of four 8 mm diameter bars, while transverse reinforcement consists of 4 mm diameter rectangular hoops spaced at 80 mm. The steel reinforcement has been designed to minimize the size effects; in fact, longitudinal reinforcement ratio is in the range of low reinforcement ratios (ρ_l = 1%), while transverse reinforcement reproduces approximately the geometrical ratio (ρ_t = 0.3%) and the spacing of a corresponding full scale element.

2.2. Material properties and strengthening systems

Yielding stress of longitudinal bars and hoops were 547 MPa and 642 MPa, respectively. Compressive strength of concrete has been evaluated by means of compressive tests on 150 mm cubes. Compressive strengths ranging between 25.7 MPa and 36.0 MPa, corre-

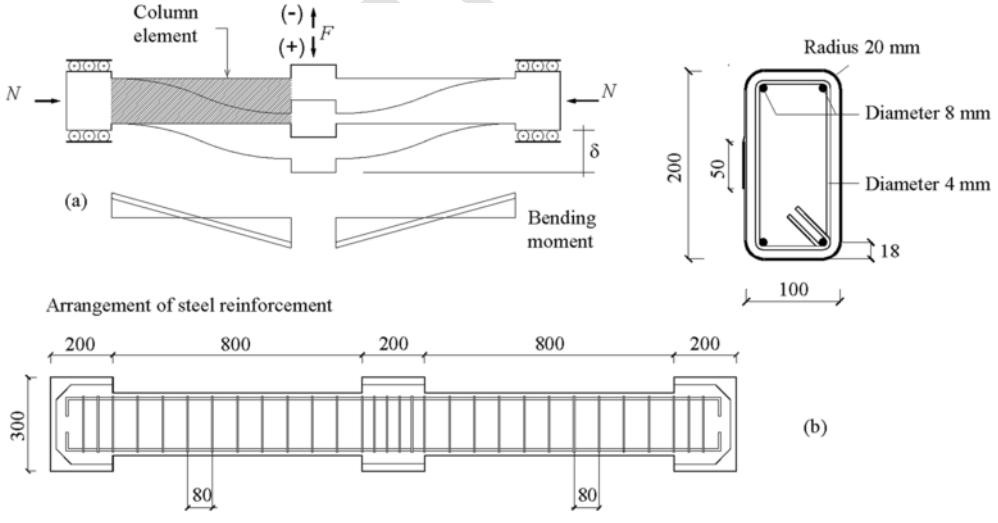

Fig. 1. (a) Test setup. (b) Arrangement of the steel reinforcement in the specimens. (Dimensions are expressed in millimeters).

sponding to cylinder strengths (f_{cm}) ranging between 21.3 MPa and 29.9 MPa, has been obtained.

The following strengthening systems have been adopted (Fig. 2).

Strengthening system type A consists of two types of CFRP sheet bonded at the ends of the column elements: a layer of balanced quadriaxial sheet was bonded to provide shear strengthening and an overlapped sheet with unidirectional fibers was wrapped to provide a passive confinement (Fig. 2a). Strengthening system type B (Fig. 2b) entails different strengthening configurations at the ends of each column element. The column end connected to the central stub were strengthened with a layer of balanced quadriaxial CFRP sheet and confined with an overlapped unidirectional CFRP sheet, while the column end connected to the end stubs were confined a unidirectional CFRP sheet only. It differs from the strengthening system A due to the lack of the quadriaxial fiber sheets at the end of the column elements connected to the end stubs. Strengthening system type C consists of a quadriaxial fiber sheet wrapped at both ends of column elements (Fig. 2c). Strengthening system type D consists of a quadriaxial FRP sheet wrapped at the end of the column elements connected to the central stub (Fig. 2d). It differs from the previous one due to the lack FRP reinforcement at the end of the column elements connected to the end stub. The properties of the two types of CFRP materials utilised for the adopted strengthening systems are summarized in Table 1; in particular, carbon fibers with high tensile strength and low modulus of elasticity have been used. The characteristics of tested specimens are listed in Table 2.

The confinement degree exerted by the adopted strengthening systems has been evaluated by the conventional value of the effective confinement lateral pressure provided by the expression [13]:

$$f_{l,eff} = k_{eff}\left(\frac{1}{2}\rho_f E_f \varepsilon_{fd,rid}\right) \tag{1}$$

where k_{eff} is an effectiveness factor depending on the shape of the wrapped cross section, ρ_f is the geometric strengthening ratio, evaluated on the basis of the fibers thickness t_f reported in Table 1, E_f is the longitudinal modulus of elasticity of the FRP material (Table 1), and $\varepsilon_{fd,rid}$ is a reduced FRP design strain, here assumed equal to 0.004. In particular, the values of 1.16 N/mm^2 and 0.46 N/mm^2 have been obtained for the unidirectional (strengthening systems A and B) and quadriaxial (strengthening systems C and D) fiber composites, respectively.

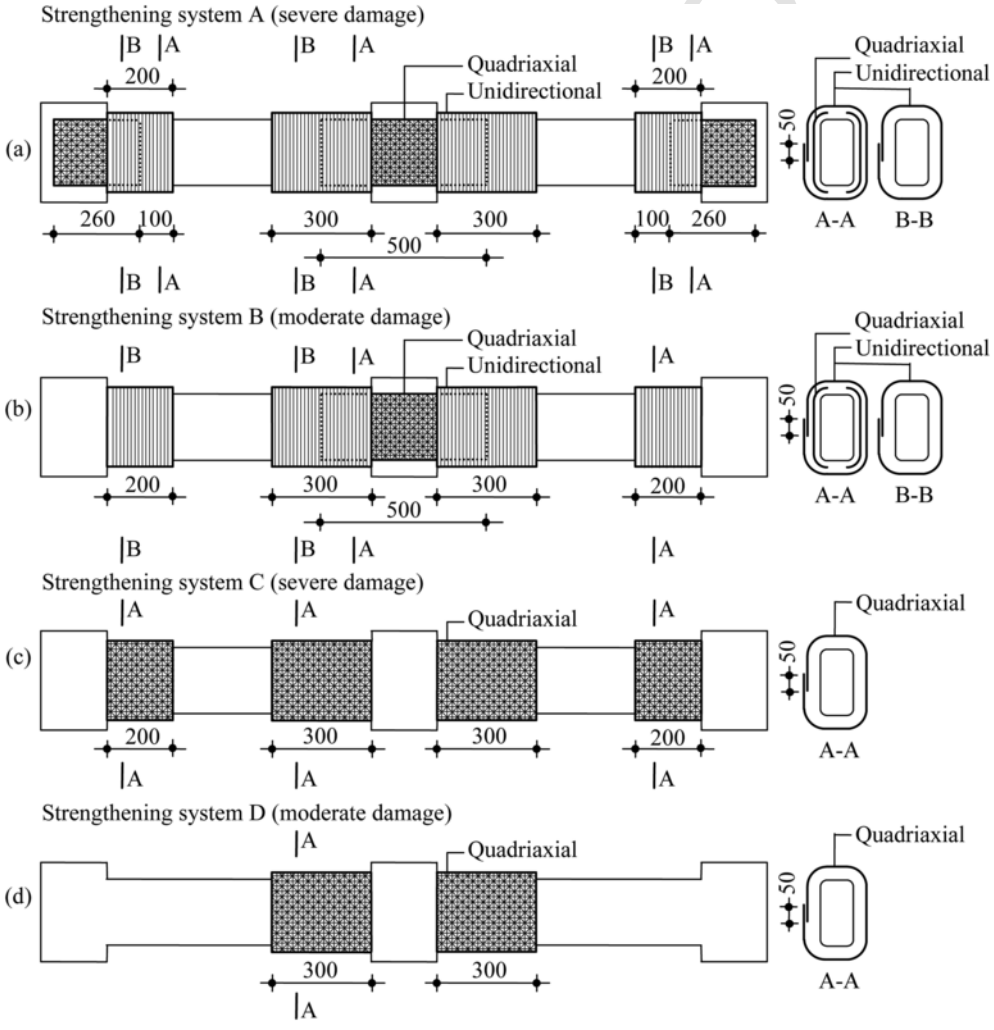

Fig. 2. Strengthening of the column ends with unidirectional and quadriaxial CFRP sheets (dimensions are expressed in millimeters).

Table 1
Properties of CFRP materials. t_f: nominal thickness. E_f: elastic modulus. f_f: tensile strength. ε_{fu}: tensile failure strain. (*) nominal thickness for each fiber direction.

CFRP sheet	t_f	E_f	f_f	ε_{fu}	Weight
	[mm]	[GPa]	[MPa]	[%]	[g/m^2]
Unidirectional	0.166	230	4830	2.0	300
Quadriaxial	0.106(*)	230	4800	2.1	760

Table 2
Characteristics of specimens. f_{cm}: concrete compressive strength. b = 100 mm and d = 200 mm are the cross-section width and depth, respectively (Fig. 1). N is the axial force applied to the column elements (Fig. 1).

Specimen	f_{cm}	$n = N/(bdf_{cm})$	Damage	Strengthening system
	[MPa]	[%]		
REF-50	27.1	9.2	–	–
REF-100	29.9	16.7	–	–
FRP50-A	28.3	8.8	severe	A
FRP50-B	26.9	9.3	moderate	B
FRP50-C	26.6	9.4	severe	C
FRP50-D	24.5	10.2	moderate	D
FRP100-A	28.7	17.4	severe	A
FRP100-B	27.6	18.1	moderate	B
FRP100-C	21.3	23.5	severe	C
FRP100-D	22.1	22.6	moderate	D

2.3. Test setup and loading sequence

Each specimen was tested in horizontal position. The axial force N (Fig. 1) was applied first. Two values of N have been considered, namely 50 kN and 100 kN , corresponding to normalized values $n=N/(bdf_{cm})$ ranging between 8.8% and 23.5% depending on the variability of the compressive strength of concrete (Table 2). Adopted values of axial load entail compressive stress levels typical of columns belonging to structures rising in areas characterized by medium-high seismic risk. Afterwards, the specimens were subjected to the alternating force F (Fig. 1) under displacement control. The axial load N was kept constant during the application of the transverse load. Cyclic transverse action has been applied according to the displacement history shown in Fig. 3.

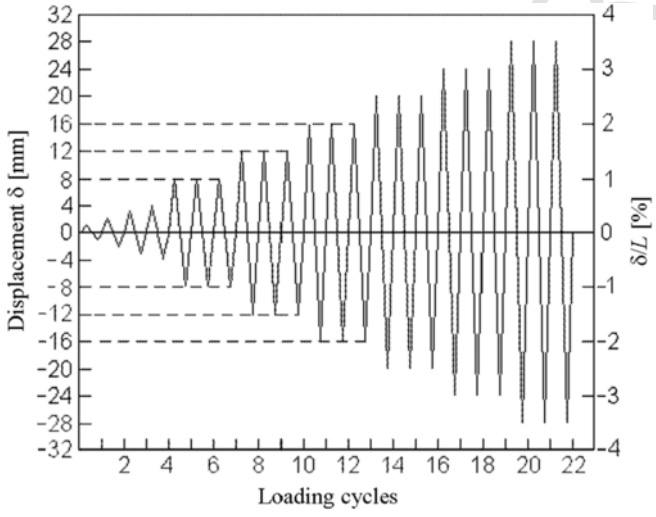

Fig. 3. Displacement history. The dotted lines correspond to the deformation levels corresponding to the initial damage.

The loading sequence has been defined in terms of element drift δ/L, being δ (Fig. 1) the transversal displacement imposed at the central stub and L = 800 mm the length of each column element. The amplitude of the drift cycles has been assumed as multiple of δ/L = 0.5%, corresponding to a conventional threshold of full operativity (fully operational limit state) for RC frame structures [28]. Each load cycle, except for the first four, has been repeated three times in order to evaluate the strength degradation. The test setup is shown in Fig. 4. Tests have been performed by means of a reaction steel frame provided with two opposite hydraulic jacks to apply the axial force and a mechanical actuator to transmit the transverse action under displacement control. Instrumentation consisted of load cells to measure applied loads (axial and transverse) and displacement transducers and strain gauges to evaluate deformations.

Two of the tested specimens, one for each level of axial force N, were used as control specimens. Therefore they were led to collapse by means of the test procedure described above. Their response has been used as a reference for the assessment of the effectiveness of the strengthening systems adopted for the remaining specimens. The remaining specimens were firstly damaged (Fig. 5a), then repaired and tested (Fig. 5b) according to the test procedure described above. The damaging procedure involved the application of the axial force N and the transverse alternating action F up to the attainment of a predetermined level of initial damage. Two levels of initial damage for each axial load have been defined on the basis of the evolution of cracking patterns observed on reference specimens (REF 50 and REF 100). In particular, the higher damage level (severe damage) has been related to the deformation level preceding the spalling of concrete cover at critical regions of column elements; such a condition corresponds to different deformations for the two values of axial load: δ/L = 2.0% (end of 13th loading cycle) for N = 50 kN and δ/L = 1.5% (end of 10th loading cycle) for N = 100 kN. The less severe damage condition (moderate damage) corresponds to δ/L = 1.5% and δ/L = 1.0% (end of 7th loading cycle) respectively for the two values of axial load.

Strengthening systems A and C were applied to the specimens subjected to severe damage, while strengthening systems B and D were applied to specimens subjected to moderate damage (Table 2). Fig. 5 shows the specimen FRP100-A at different testing phases: damage condition preceding the application of the CFRP materials (Fig. 5a) and repaired condition (Fig. 5b). Fig. 6 shows the specimen FRP50-C after the application of the quadriaxial CFRP sheets.

The tested specimens are summarized in Table 2. In this table the names of the repaired specimen are of the type FRPX-Y, where X is the axial load applied in kN and Y (=A, B, C, or D) indicates the type of strengthening system applied.

In this investigation, a rotational release has been produced at the concrete stubs connected to the reaction frame, whereas a condition of fixed rotation was imposed at the central stub due to the structural symmetry. Thus, the end cross-sections of each column element were subjected to different values of bending moment and, as a consequence, a different damage intensity resulted at critical regions of the same column element. In particular, the critical zones adjacent to the central stub evidenced a higher level of damage than the critical zones adjacent to the end stubs.

3. Test results and discussion

The failure of all the repaired specimens was caused by the debonding of the CFRP material from the substrate. The detachment of the composite materials happened due to the formation of an interfacial crack within the concrete (cohesive debonding), as shown in

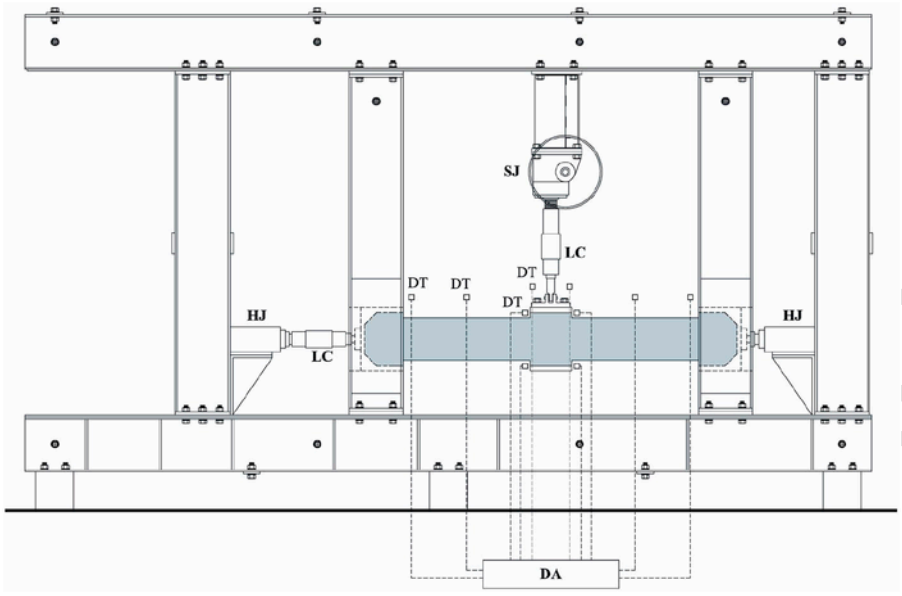

Fig. 4. Test setup (HJ: hydraulic jack; SJ: screw jack; LC: load cell; DT: displacement transducer; DA: data acquisition and elaboration system).

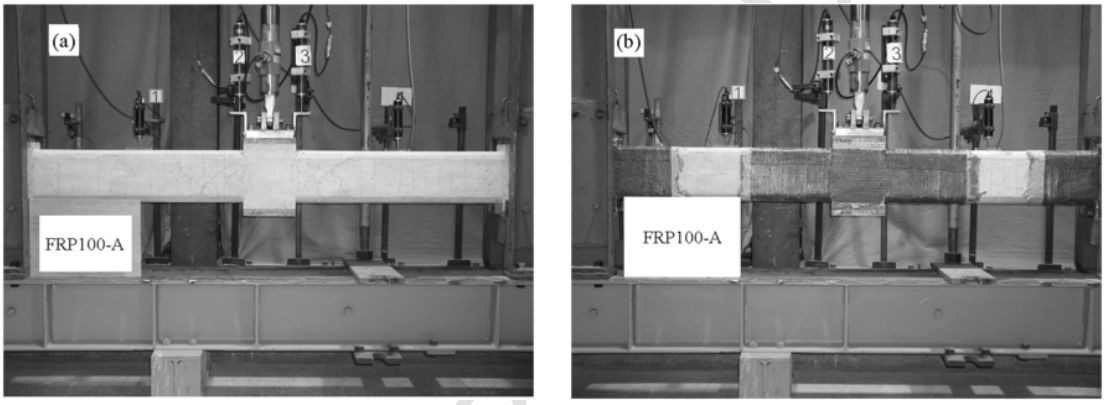

Fig. 5. Specimen FRP100-A (a) after the damaging and (b) after the repair intervention.

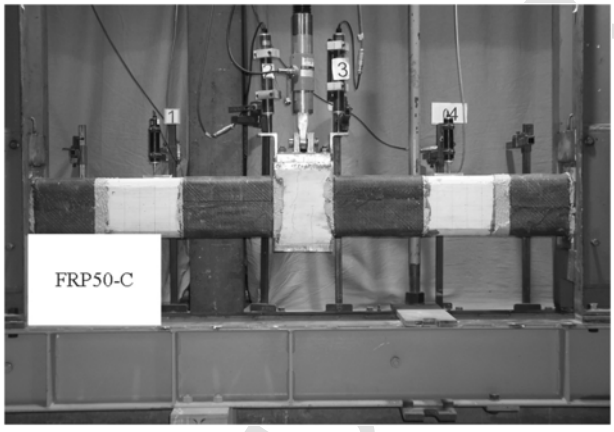

Fig. 6. Specimen FRP50-C after the application of the quadriaxial CFRP sheet.

Fig. 7, where the fracture surface is shown. This failure mode is typical for FRP strengthened RC and masonry structures, as pointed out by many authors ([7,9,10,11,13,21-25]).

3.1. Load-displacement curves

Test results are presented herein in terms of load-displacement curves; these curves show the force F applied at the central stub plotted as a function of the displacement δ imposed to the same stub (Fig. 1). Remarks on stiffness degradation and energy dissipation of tested specimens are also made.

Figs. 8 and 9 show the load-displacement curves of reference unstrengthened specimens (REF50, $N = 50$ kN and REF100, $N = 100$ kN). Figs. 10 and 11 show details of the damage suffered by these specimens during the tests.

The cyclic response of specimen REF50 ($n = 9.2\%$) was characterized by sufficiently stable hysteresis loops up to the deformation level $\delta/L = 3.5\%$ (end of the 19th loading cycle) with a moderate strength degradation up to the 16th loading cycle. A higher strength degradation (13%) can be observed for the last three loading cycles (Fig. 8). The response curve presented a marked pinching due to the influence of the shear mechanisms on specimen response. The failure of the specimen was attained at beginning of the 21st cycle because of the rupture of a longitudinal rebar. The examination of the speci-

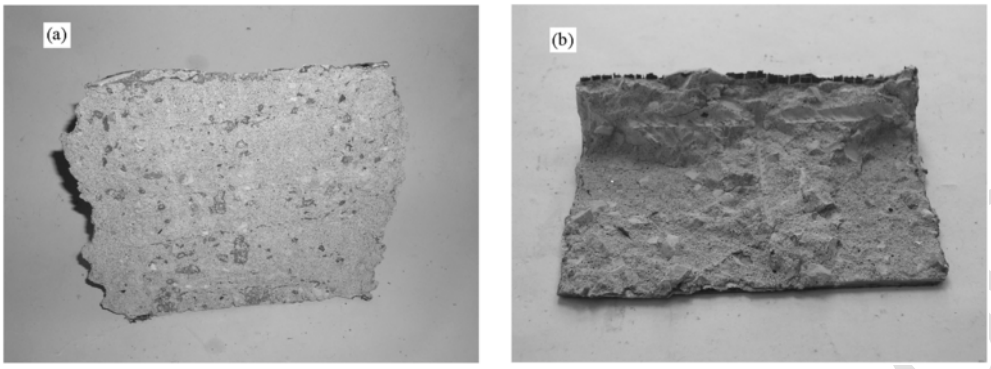

Fig. 7. Detachment of FRP materials: (a) at a nodal surface; (b) at a critical region.

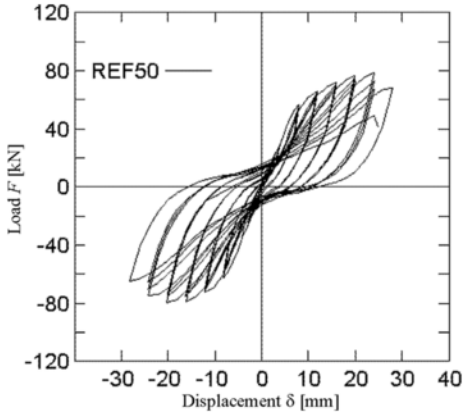

Fig. 8. Load-displacement curve of control specimen REF50 (N = 50 kN).

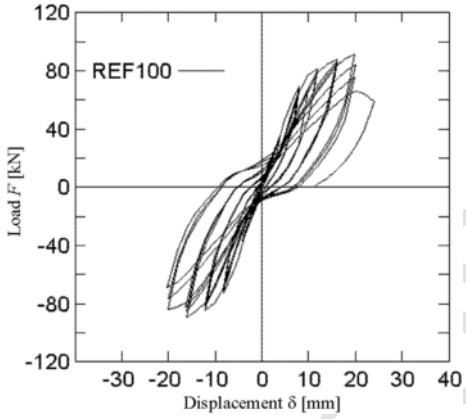

Fig. 9. Load-displacement curve of control specimen REF100 (N = 100 kN).

men after test pointed out a remarkable concrete degradation near the central stub (Fig. 10) and the buckling of longitudinal bars.

As expected, the untrengthened specimen REF100 (n = 16.7%) exhibited a greater strength and a lower deformation capacity than the specimen REF50. Hysteresis loops were less stable with considerable strength degradation, especially at high deformation levels (Fig. 9). Failure was reached at beginning of the 17th cycle due to the overall instability of the specimen caused, in turn, by the excessive concrete degradation and buckling of longitudinal bars at critical regions (Fig. 11).

Figs. 12 and 13 show the load-displacement curves of specimens subjected to initial damaging and then repaired with the strengthening

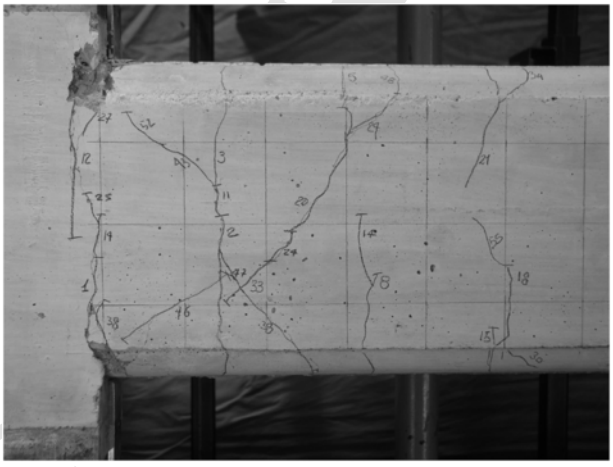

Fig. 10. Specimen REF50: cracking pattern at a critical region.

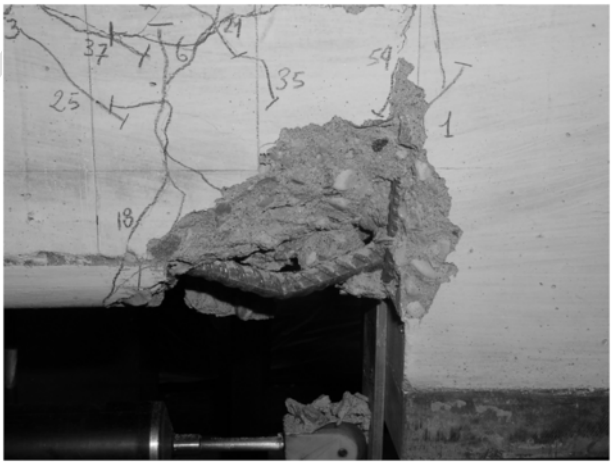

Fig. 11. Specimen REF100: buckling of a longitudinal bar at a critical region.

systems previously described: strengthening systems A, B obtained by combining unidirectional and quadriaxial CFRP sheets (specimens FRP50-A, B and FRP100-A, B), and strengthening systems C, D obtained with quadriaxial CFRP sheets only (specimens FRP50-C, D and FRP100-C, D). In order to emphasize effects of the application of the CFRP materials, response curves of repaired specimens have been superimposed to curves of the companion, i.e. subjected to the same axial force, reference specimens.

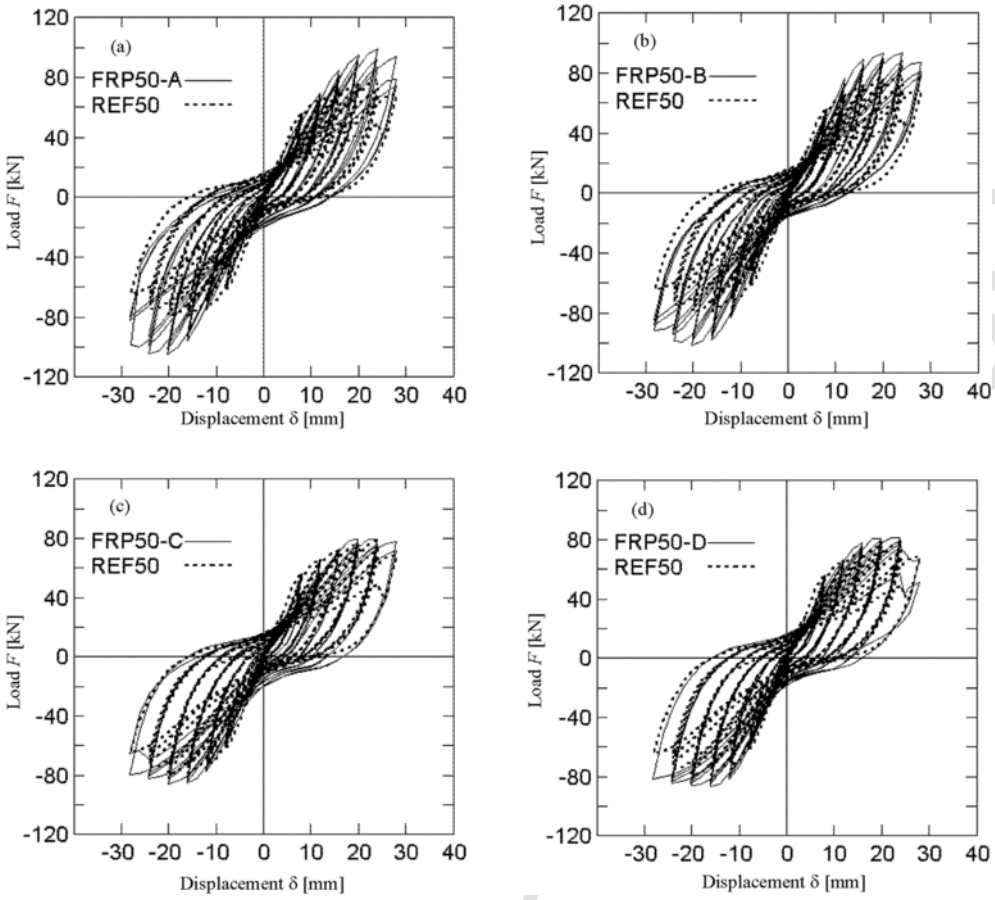

Fig. 12. Comparison between the load-displacement curves of the repaired specimens subjected to the axial force $N = 50$ kN and the companion unstrengthened specimens. (a) strengthening system A. (b) strengthening system B. (c) strengthening system C. (d) strengthening system D.

Examination of the response curves relative to the repaired specimens subjected to $N = 50$ kN, ($n \cong 10\%$) shows that the strengthening systems A and B (combination of unidirectional and quadriaxial sheets) produced a greater benefit than the strengthening systems C and D, both in terms of strength and deformation capacity (Fig. 12).

In particular, the specimen FRP50-A, characterized by a considerable initial damage level, has gained an increase of strength of about 29% with respect to the control specimen REF50. Besides, a moderate strength degradation was caused by the repeated cycles, except for the last three cycles (corresponding to a deformation level of $\delta/L = 3.5\%$) for which strength degradation was equal to 20%. Specimen FRP50-B, which started from a less severe damage condition, exhibited similar performances, with a strength increase of 22% and a smaller strength degradation (9%).

For specimens subjected to $N = 50$ kN and repaired with the strengthening systems C and D (quadriaxial sheets only), beneficial effects of the external reinforcement were less evident. In particular, these specimens showed a lower deformation capacity ($\delta/L = 3.0\%$) than specimens repaired with the strengthening systems A and B because of the rupture of longitudinal bars due to excess of tension occurred at critical regions. However, response curves of these specimens pointed out a good capacity to recover mechanical properties, with strength increases of 4% and 11% with respect to the control specimen for specimens FRP50-C and FRP50-D, respectively. Mechanical degradation at the maximum deformation level was of 17% (FRP50-C) and 5% (FRP50-D).

Cyclic responses of specimens subjected to $N = 100$ kN ($n \cong 20\%$) showed, among them, less marked differences with respect to specimens subjected to $N = 50$ kN. In fact, they attained the same deformation level at failure ($\delta/L = 3.0\%$), showing however some differences in their response. In particular, specimens repaired with unidirectional and quadriaxial CFRP sheets (FRP100-A and FRP100-B) obtained significant increases in strength (25% and 24% respectively) with respect to the companion control specimen. However, this outcome was accompanied by a considerable mechanical degradation (12% and 9%, respectively) and quite narrow hysteresis loops. Specimens repaired with quadraxial sheets only (FRP100-C and FRP100-D), while gaining lower increases in strength (9% and 10% respectively), exhibited more stable hysteresis loops and a lower strength degradation (7% and 5%, respectively).

3.2. Stiffness degradation and hysteresis energy

The experimental response of tested specimens in terms of stiffness degradation during the loading cycles is shown in Fig. 14. The stiffness associated to each cycle has been evaluated by averaging stiffness associated to the two semi-cycles, obtained, in turn, as the ratio of the maximum load to the corresponding displacement.

In particular, Fig. 14a refers to the specimens with $N = 50$ kN.

This figure shows that in the initial part of the loading process the stiffness of the repaired specimens was lower than that characterizing the companion reference specimen, since the repaired specimens start out from a damaged condition. At higher deformation levels (about

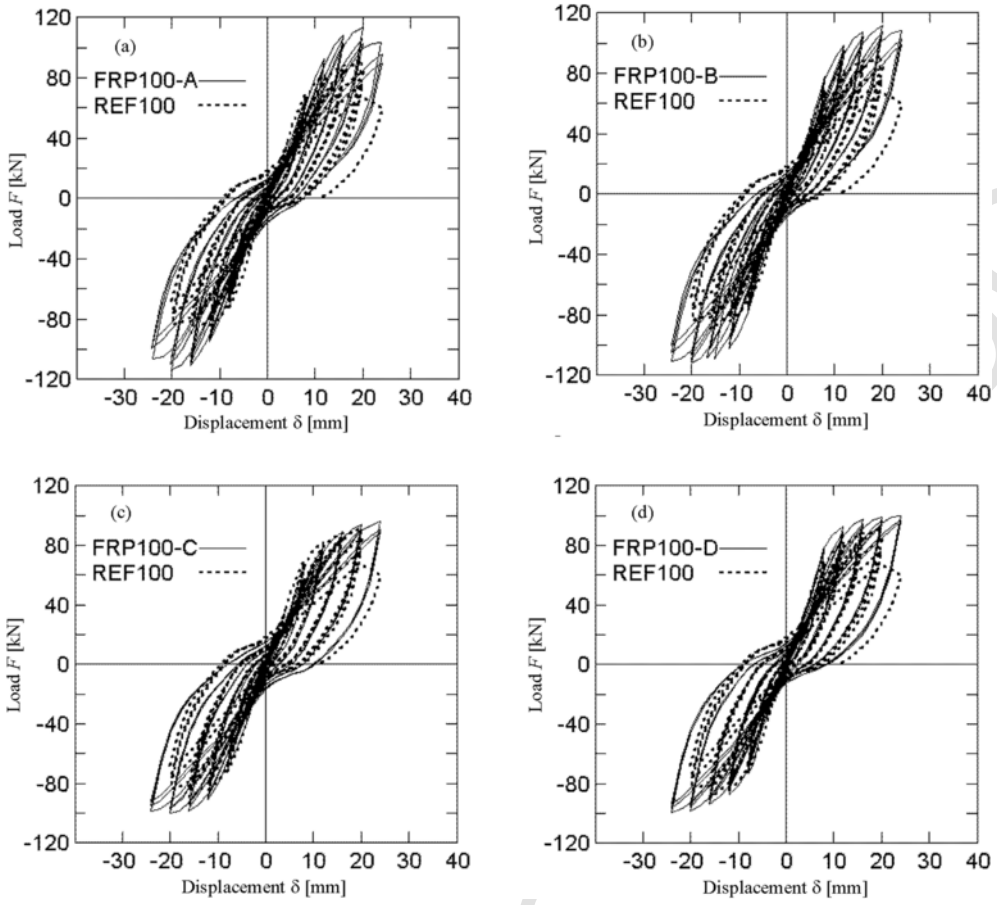

Fig. 13. Comparison between the load-displacement curves of the repaired specimens subjected to the axial force $N = 100$ kN and the companion unstrengthened specimens. (a) strengthening system A. (b) strengthening system B. (c) strengthening system C. (d) strengthening system D.

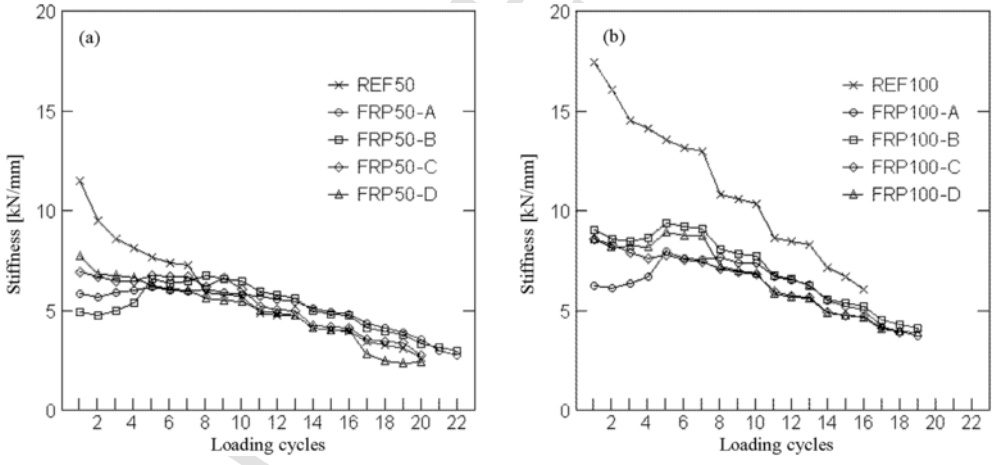

Fig. 14. Stiffness decrease during the cyclic tests. (a) Specimens with $N = 50$ kN. (b) Specimens with $N = 100$ kN.

the 8th cycle) this trend is reversed, since the stiffness of repaired specimens becomes higher than the stiffness of the control specimen. This confirms the effectiveness of the strengthening material for the limitation of the damages produced by the cyclic loading. No substantial differences have been noticed among responses of repaired specimens FRP50-A, B, C, and D.

In the case of specimens subjected to the axial compression of 100 kN (Fig. 14b), the stiffness of the repaired specimens is always lower than the stiffness of the control specimen. This means that the applied CFRP composites were not able to completely recover the initial damage imposed to the specimens. Nonetheless, the stiffness of the repaired and unstrengthened specimens tends to attain similar values at high deformation rates. In both series ($N = 50$ kN and $N = 100$ kN) it is observed that specimens repaired with strengthening systems A and B reach failure conditions with higher stiffness than specimens repaired with strengthening systems C and D.

The experimental response of tested specimens in terms of energy dissipation is shown in Fig. 15, where the total hysteresis energy dissipated at the generic i-th cycle is plotted. Fig. 15a refers to the specimens subjected to $N = 50$ kN, while Fig. 15b refers to the specimens subjected to $N = 100$ kN. It can be seen that repaired specimens exhibit a greater dissipation capacity with respect to control specimens, especially at medium-high deformation levels. Better results are obtained by specimens repaired with quadriaxial sheets only (FRP50-D and FRP100-D). This outcome is probably due to the ability of the quadriaxial sheet to bridge the inclined shear cracks.

4. Conclusions

This paper presents results of an experimental investigation, developed at the Laboratory LUPM of the University of Florence, aimed at studying cyclic response of RC elements previously damaged and then repaired with CFRP composites. Ten specimens representing half scale rectangular RC columns were tested; two of them were tested without FRP strengthening (control specimens) in order to provide a reference for assessing behavior of repaired specimens. Study variables were the level of initial damage, the type of external reinforcement and the intensity of axial load. Repaired specimens have been subjected, before the application of the strengthening material, to two damage levels, severe and moderate. Two strengthening systems were applied to the tested specimens depending on the level of damage. Test results have pointed out effectiveness of the tested strengthening systems since repaired specimens exhibited better mechanical performances if compared to companion unstrengthened specimens. The FRP materials bonded at critical regions prevented spalling of concrete cover, buckling of longitudinal bars and an excessive damage of concrete. As a consequence repaired specimens were capable to sustain a greater number of loading cycles with respect to control specimens. This outcome was more evident for specimens repaired by strengthening systems with unidirectional and quadriaxial carbon fiber sheets. In fact, these specimens exhibited an increase of strength ranging from 22% to 29%, while specimens repaired with quadriaxial sheets only exhibited an increase of strength ranging from 4% to 10%. The application of unidirectional and quadriaxial sheets produced also a greater deformation capacity than the application of quadriaxial sheets only. This is due to a more effective protection of critical regions exerted by the system combining unidirectional and quadriaxial fiber sheets; in particular these latter give a contribution to the absorption of tensile forces within longitudinal bars, in addition to the function of stitching concrete cracks. Conversely, specimens reinforced by quadriaxial fiber sheets only revealed a better dissipation capacity due to their capacity to oppose shear mechanisms. Concerning the effects of the axial compression levels, test results pointed out that specimens which took greater advantage of the adopted reinforcing systems were the ones subjected to the higher value of axial force. No evident effects were recognized in relation to the asymmetry of reinforcement applied to end regions of the single column elements. Finally, it is the opinion of the authors that the problem of recovering stiffness in repaired columns should be addressed with particular attention because of the importance that stiffness plays in the force distribution within the structures, subject to seismic actions.

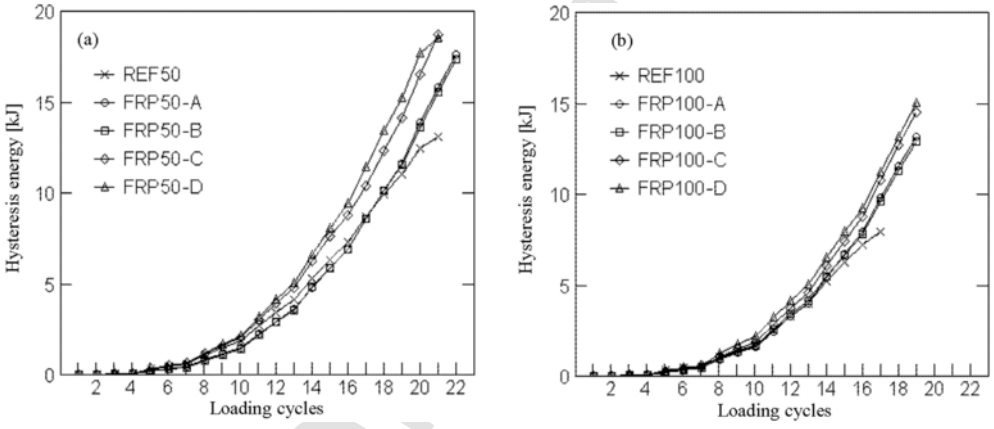

Fig. 15. Hysteresis energy during the cyclic tests. (a) Specimens with $N = 50$ kN. (b) Specimens with $N = 100$ kN.

References

[1] A. Ghobarah, T.S. Aziz, A. Biddah, Rehabilitation of reinforced concrete frame connections using corrugated steel jacketing, ACI Struct J 4 (3) (1997) 283–294.

[2] A. Biddah, A. Ghobarah, T.S. Aziz, Upgrading of nonductile reinforced concrete frame connections. Journal of structural engineering, ASCE 123 (8) (1997) 1001–1009.

[3] S.M. Alcocer, J.O. Jirsa, Strength of reinforced concrete frame connections rehabilitated by jacketing, ACI Struct J 90 (3) (1993) 249–261.

[4] J.M. Bracci, A.M. Reinhorn, J.B. Mander, Seismic retrofit of reinforced concrete buildings designed for gravity loads: Performance of structural model, ACI Struct J 92 (6) (1995) 711–723.

[5] S. Hakuto, R. Park, H. Tanaka, Seismic load tests on interior and exterior beam-column joints with substandard reinforcing details, ACI Struct J 97 (1) (2000) 11–25.

[6] A.G. Tsonos, Seismic repair of exterior R/C beam-to-column joints using two-sided and three-sided jackets, Struct Eng Mech 13 (1) (2002) 17–34.

[7] J.G. Teng, J.F. Chen, S.T. Smith, L. Lam, FRP: strengthened RC structures, John Wiley & Sons, Ltd, Chichester, UK, 2001.

[8] L. Rovero, F. Focacci, G. Stipo, Structural behavior of arch models strengthened using fiber-reinforced polymer strips of different lengths, J Comp Const 17 (2) (2013) 249–258.

[9] F. Focacci, C. Carloni, Periodic variation of the transferable load at the FRP-masonry interface, Compos Struct 129 (2015) 90–100.

[10] C. Carloni, F. Focacci, FRP-masonry interfacial debonding: An energy balance approach to determine the influence of the mortar joints, Eur J Mech A/Solids 55 (2016) 122–133.

[11] M. Malena, F. Focacci, C. Carloni, G. de Felice, The effect of the shape of the cohesive material law on the stress transfer at the FRP-masonry interface, Compos Part B 110 (2017) 368–380.

[12] A. D'Ambrisi, F. Focacci, R. Luciano, Experimental investigation on flexural behavior of timber beams repaired with CFRP plates, Comp Struct 108 (2014) 720–728.

[13] CNR DT-200 R1/2013, Guide for the design and construction of externally bonded FRP systems for strengthening existing structures, 2013. [Consiglio Mazionale delle Ricerche, Roma, Italy.].

[14] Japan Society of Civil Engineering (JSCE), Reccomandations for upgrading of concrete structure with use of continuous fiber sheets, Tokyo, Japan Concr Eng Ser 41 (2001).

[15] American Concrete Institute (ACI), Guide for the design and construction of externally bonded FRP systems for strengthening concrete structures, 2008. ACI 440.2R-08, Farmington Hills, MI.

[16] Féderation Internationale du Béton (FIB), Externally bonded FRP reinforcement for RC structures, Bulletin 14 (2001). [Lausanne, Switzerland].

[17] A. Ghobarah, A. Said, Shear strengthening of beam-column joints, Eng Struct 24 (2002) 881–888.

[18] T. El-Amoury, A. Ghobarah, Seismic rehabilitation of beam–column joint using GFRP sheets, Eng Struct 24 (2002) 1397–1407.

[19] B. Li, Q. Kai, Seismic behavior of reinforced concrete interior beam-wide column joints repaired using FRP, J Compos Constr 15 (5) (2011) 327–338.

[20] A. Balsamo, A. Colombo, G. Manfredi, P. Negro, A. Prota, Seismic behavior of a full-scale RC frame repaired using CFRP laminates, Eng Struct 27 (2005) 769–780.

[21] C. Carloni, K.V. Subramaniam, Direct determination of cohesive stress transfer during debonding of FRP from concrete, Comp Struct 93 (2010) 184–192.

[26] C.P. Antonopoulos, T.C. Triantafillou, Experimental investigation of FRP-strengthened RC beam-column joints, J Compos Constr 7 (1) (2003) 39–49.

[27] Nudo R. Inelastic response of HSC elements under transverse loading. Proc. 4th International Conference on Seismology and Earthquake Engineering. Tehran, Iran; 2003.

[28]Structural Engineers Association of California (SEAOC), Blue Book. Preliminary guidelines for performance based seismic engineering. Part 2, Sacramento, USA 1998.